HHS Public Access

Author manuscript

FASEB J. Author manuscript; available in PMC 2023 July 01.

Published in final edited form as:

FASEB J. 2022 July ; 36(7): e22390. doi:10.1096/fj.202101855RRR.

Acyl-CoA:wax alcohol acyltransferase 2 modulates the cone visual cycle in mouse retina

Made Airanthi K. Widjaja-Adhi[1,#],

Alexander V. Kolesnikov[2,#],

Sreelakshmi Vasudevan[3],

Paul S.-H. Park[3],

Vladimir J. Kefalov[2,4,*],

Marcin Golczak[1,5,*]

[1]Department of Pharmacology, School of Medicine, Case Western Reserve University, Cleveland, OH;

[2]Department of Ophthalmology, Gavin Herbert Eye Institute, University of California, Irvine, CA.

[3]Department of Ophthalmology and Visual Sciences, School of Medicine, Case Western Reserve University, Cleveland, OH;

[4]Department of Physiology and Biophysics, University of California, Irvine, CA.

[5]Cleveland Center for Membrane and Structural Biology, School of Medicine, Case Western Reserve University, Cleveland, OH;

Abstract

The daylight and color vision of diurnal vertebrates depends on cone photoreceptors. The capability of cones to operate and respond to changes in light brightness even under high illumination is attributed to their fast rate of recovery to the ground photosensitive state. This process requires the rapid replenishing of photoisomerized visual chromophore (11-*cis*-retinal) to regenerate cone visual pigments. Recently, several gene candidates have been proposed to contribute to the cone-specific retinoid metabolism, including acyl-CoA wax alcohol acyltransferase 2 (AWAT2, aka MFAT). Here, we evaluated the role of AWAT2 in the regeneration of visual chromophore by the phenotypic characterization of *Awat2*$^{-/-}$ mice. The global absence of AWAT2 enzymatic activity did not affect gross retinal morphology or the rate of visual chromophore regeneration by the canonical RPE65-dependent visual cycle. Analysis of *Awat2*

[*]To whom the correspondence should be addressed: Marcin Golczak, Ph.D., Department of Pharmacology, School of Medicine, Case Western Reserve University, 10900 Euclid Ave, Cleveland, Ohio 44106, USA; Phone: 216-368-0302; mxg149@case.edu, Vladimir J. Kefalov, Ph.D., Department of Ophthalmology, University of California Irvine, 2121 Gillespie|837 Health Sciences Rd., Irvine, CA 92697, USA; Phone: (949) 824-0552; vkefalov@uci.edu.

[#]These authors contributed equally to this work.

AUTHOR CONTRIBUTION

M.A.K.W.A., A.V.K., P.S.H.P, V.J.K., and M.G. designed the experiments. M.A.K.W.A., A.V.K., S.V., and M.G. performed the experiments and collected the data. All authors analyzed the data and contributed intellectually to their interpretation. M.A.K.W.A., A.V.K., V.J.K., and M.G. wrote the manuscript with valuable input from all other authors.

CONFLICT OF INTEREST

The authors declare that they have no competing interests.

expression indicated the presence of the enzyme throughout the murine retina, including the retinal pigment epithelium (RPE) and Müller cells. Electrophysiological recordings revealed reduced maximal rod and cone dark-adapted responses in AWAT2-deficient mice compared to control mice. While rod dark adaptation was not affected by the lack of AWAT2, M-cone dark adaptation both in isolated retina and *in vivo* was significantly suppressed. Altogether, these results indicate that while AWAT2 is not required for the normal operation of the canonical visual cycle, it is a functional component of the cone-specific visual chromophore regenerative pathway.

Keywords

AWAT2; MFAT; cone visual cycle; visual chromophore; dark adaptation

INTRODUCTION

The sensory perception of visual images in vertebrates depends on two types of specialized neurons, rods and cones (1–3). Rods are highly sensitive to light, supporting monochromatic vision under dim-light conditions. However, their signals become saturated at a relatively low threshold, limiting rod contribution to vision at daytime, photopic, light intensities. In contrast, cones are typically 100 times less sensitive to light and enable the perception of colors (4–6). They possess a very high saturation threshold that allows them to function under bright light conditions. On the molecular level, the detection of light is initiated when photons that reach the retina are absorbed by an 11-*cis*-retinal (11cRAL) molecule (visual chromophore) coupled covalently to G protein-coupled receptor scaffolds called opsins (7, 8). The light-induced isomerization of the 11-*cis*-retinylidene moiety to its all-*trans* configuration causes the activation of the receptors that triggers phototransduction signaling. To sustain the photosensitivity of photoreceptors, it is necessary to replenish the photoisomerized 11cRAL molecules. This is mainly achieved by the light-independent enzymatic pathway known as the canonical visual cycle that occurs in the photoreceptors and the retinal pigment epithelium (RPE) (9). It utilizes the catalytic activities of two non-redundant enzymes lecithin:retinol acyltransferase (LRAT) and retinal pigment epithelium-specific 65 kDa protein (RPE65) (10–13). The canonical visual cycle serves as a major source of visual chromophore for rods and also contributes to the regeneration of cone visual pigments (14–16). However, because of the discrepancies between the rates of RPE65-depenent production of 11cRAL and the several times faster dark adaptation of cones under strong light illumination, it has been proposed that cones utilize an alternative source of readily accessible visual chromophore (17, 18).

The early evidence supporting the existence of a cone-specific visual cycle comes from studies on Muller glia-expressed cellular retinaldehyde-binding protein (CRALBP) (19). The electrophysiological evaluation of CRALBP-deficient mice provided early indication for the important role of this protein in cone dark adaptation (19, 20). The independent functional screening of genetic DNA libraries from Muller cells led to the identification of two enzymes: sphingolipid delta4 desaturase 1 (DES1) and acyl-CoA wax alcohol acyltransferase 2 (AWAT2, aka multifunctional O-acyltransferase or MFAT) as potential retinoid-processing proteins involved in an intraretinal metabolic pathway yielding 11cRAL

(21, 22). Both enzymes exhibit substrate promiscuity and are known to be involved in metabolic pathways leading to the biosynthesis of ceramides and long chain alcohol esters respectively (23, 24). Recent *in vitro* experiments suggested that DES1 could catalyze the equilibrium isomerization of all-*trans*-retinol (21). The enzymatic activity of DES1, coupled with the esterification of *cis*-retinols catalyzed by AWAT2 resulted in an accumulation of 11-*cis*-retinyl esters, a storage form of *cis* retinoids and precursor of 11cRAL readily detectable in cone-dominant retinas (Fig. 1A) (22). However, despite these observations, recently provided genetic evidence does not support the stipulated function of DES1 in the regeneration of visual chromophore. The selective elimination of DES1 from the Muller cells did not affect the rate of cone dark adaptation in mice (25). Similarly, the deactivation of the orthologous gene degs1 in zebrafish also did not alter cone function (26).

The role of AWAT2 in ocular retinoid metabolism remains unknown and the fact that DES1 expression in Müller glia is not required for the regeneration of cone visual pigment, does not necessarily implicate functional insignificance of AWAT2 for ocular retinoid metabolism. The enzymatic assays performed *in vitro* indicate its ability to facilitate the robust acyl-CoA-dependent esterification of numerous lipid substrates, including long chain alcohols, mono- and diacylglycerols, as well as retinol, with a high substrate specificity towards *cis*-isomers (27–29). The recent characterization of *Awat2*$^{-/-}$ mice confirmed the non-redundant role of this enzyme in the biosynthesis of wax esters, the main component of the meibum (30). Consequently, the absence of AWAT2 activity resulted in a suboptimal lipid composition of the meibum, instability of the lipid tear film, and symptoms of obstructive dry eye disease (30). However, the substrate promiscuity may indicate tissue-specific functions of AWAT2. To investigate the proposed role of this enzyme in the cone-specific regeneration of visual chromophore, we examined whether *Awat2*$^{-/-}$ mice reveal impairments in retinal structure, cone-driven light responses, or cone dark adaptation.

MATERIAL AND METHODS

Animal genetic manipulation and genotyping

All mice used in this study were housed in the pathogen-free animal facility at the School of Medicine, Case Western Reserve University, where they were maintained under a 12-h light/12-h dark cycle (~50 lux) environment with food and water available *ad libitum*. All animal procedures and experiments were approved by the Case Western Reserve University Animal Care Committee and conformed to both the recommendations of the American Veterinary Medical Association Panel on Euthanasia and the Association of Research for Vision and Ophthalmology.

The generation of the genetically modified mouse line with the *loxP* and *loxP*/FRT flanking exons 3, 4, and 5 of the *Awat2* gene was subcontracted to the InGenious Targeting Laboratory (30). The *Awat2*-knockout mice (*Awat2*$^{-/-}$) were generated by the deletion of a portion of the *Awat2* gene using the *cre/loxP* recombination system. For this purpose, Awat2-LoxP hemizygotes (*Awat2*$^{fl/Y}$) mice were crossed with female *Sox2-cre* transgenic mice (B6-Cg-Tg(Sox2-cre)1Amc/J from The Jackson Lab (Stock# 008454) (30–32). To allow isolation of the electrophysiological response of cone photoreceptors, female non-carrier Sox2-cre *Awat2*$^{-/-}$ (homozygous females) and male non-carrier Sox2-cre *Awat2*$^{-/Y}$

(hemizygous males) were crossbred with B6.Cg-*Gnat1*^{irdr}/Boc (*Gnat1*^{irdr}) mice that contain spontaneous mutation in the guanine nucleotide-binding protein subunit α transducing 1 (*Gnat1*) gene (The Jackson Lab, Stock# 008811) (33). Genotyping was conducted by genomic PCR using the primers SC1, SDL2, and NDEL2 for the *Awat2* gene and 15495, oIMR6082, oIMR7338, oIMR7339 for *Sox2-cre* as described previously (30). The presence of *Gnat1*^{irdr} mutation was verified by PCR using the following primers: rd17-F (5'-CTCAGAATACCAGCTCAATG-3') and rd17-R (5'-GCTCTAGGTCTGAGAGATAG-3') (Fig. 1B).

Acyl-CoA-dependent long chain alcohols esterification assay

The acyltransferase activity of AWAT2 was examined in microsomes isolated from homogenized skin samples of WT and *Awat2*$^{-/-}$ mice by adapting the procedure described in Arne et al. (29). Microsomes (50 μg of total protein) were incubated with 0.1 mM tetradecanol and 0.4 mM myristoyl-CoA in 20 mM Tris/HCl buffer (pH 8.0). The alcohols were delivered in 2 μl of *N,N*-dimethylformamide. The total volume of the reaction mix was 0.2 mL. The enzymatic reaction was carried out at 37 °C with moderate shaking in an Eppendorf thermomixer (600 rpm) for 1 h and stopped by the addition of 0.2 ml of ethanol. To quantify the reaction product (myristyl myristate) by LC/MS, 400 pmol of external standard, palmityl myristate (Cayman Chemicals) were added to each sample prior to extraction with 0.3 ml of hexane. The samples were centrifuged at 15,000 × g to separate the hexane phase. To analyze the alcohol ester content of the extracts, 100 μL from each sample were injected onto a Luna PREP silica column (250 × 4.6 mm, 10 μm, Phenomenex). The alcohol esters were eluted with an isocratic flow of 1% ethyl acetate (v/v) in hexane at a flow rate of 1.5 mL/min. The eluent was directed into an LTQ linear ion trap mass spectrometer (Thermo Scientific) via an atmospheric pressure chemical ionization source working in the positive mode. The amount of myristyl myristate was quantified by comparing the areas under ion intensity peaks for the standard (m/z = 453.3 $[M+ H]^+$) and the product of the enzymatic reaction (m/z = 425.3 $[M+ H]^+$) (29).

Retinols esterification assay

The Acyl-CoA-dependent esterification of retinol was examined in homogenates obtained from retinas isolated from WT and *Awat2*$^{-/-}$ mice. Retinas from 4–5 mice were pooled together, washed with ice-cold phosphate-buffered saline (PBS) twice and homogenated in a glass-glass homogenator. The homogenates (150 μg of total protein) were incubated with 2 μM of 11-*cis*-retinol and all-*trans*-retinol in the presence of 0.4 mM myristoyl-CoA (C14:0-CoA) and 1% (m/v) bovine serum albumin in PBS. The total volume of the reaction mix was 0.2 mL. To control for potential contamination of the assay with RPE-derived LRAT activity, the control samples were incubated without the addition of acyl-CoA. After incubated at 30 °C with moderate shaking (600 rpm) for 1 h, the enzymatic reactions were stopped by the addition of 0.2 mL of ethanol followed by the extraction of the retinoids with 0.3 mL of hexane. The retinoid compositions in the hexanoic extracts were examined by normal phase HPLC. Retinoids were separated on a Luna PREP silica column (250 × 4.6 mm, 10 μm) column in a step gradient of ethyl acetate in hexane (1% for 10 min followed by 10% for additional 20 min at a flow rate of 1.5 ml/min). Individual classes of retinoids were detected at the wavelengthss of 318 nm and 325 nm and identified based on their retention

time and characteristic UV/Vis spectra. The quantification of retinyl esters was performed based on the standard curves that correlate the amount of synthetic standards and the area under the corresponding chromatography peaks.

HPLC analysis of ocular retinoid

To measure the recovery of 11-*cis*-retinal after photobleaching, 12-week-old mice were anesthetized by intraperitoneal injection of 0.2 ml/25 g body weight of a mixture containing 20 mg/ml ketamine and 1.75 mg/ml xylazine in phosphate-buffered saline. Pupils of mice were dilated with a mixture of 0.5% tropicamide and 0.5% phenylephrine hydrochloride (Santen Pharmaceutical) and mice were exposed to 15,000 lux white light for 5 min. Mice were then moved to a darkroom and euthanized at the appropriate time points. Eyes were enucleated and homogenated in 1 mL of a mixture of PBS and ethanol (50%/50%, v/v) containing 40 mM hydroxylamie. After 20 min incubation at room temperature, retinoids were extracted with 5 mL of hexane. The organic phase was collected and evaporated in a SpeedVac. Retinoid separation and quantification were performed as described previously (34). Retinoids were separated by normal-phase HPLC using 1100 series instrument (Agilent Technology) and a Luna PREP silica column (250 × 4.6 mm, 10 μm) column in a step gradient of ethyl acetate in hexane (1% for 10 min followed by 10% for additional 20 min at a flow rate of 1.5 ml/min). Individual classes of retinoids were detected at the wavelengths of 325 nm and 360 nm. 11-*cis*-Retinal was quantified according to the standard curves that correlate the amount of injected synthetic standard and the area under its chromatography peak.

Spectral Domain Optical Coherence Tomography (SD-OCT)

The morphology of the retina was examined by SD-OCT (Envisu R2210, Bioptigen). For *in vivo* imaging, mice were anesthetized with a ketamine/xylazine cocktail and the pupils dilated as described above. The retinal imaging was performed and the acquired raw data were examined using Envisu application software.

Immunofluorescence staining

Mouse eyes were collected and immediately fixed in 4% paraformaldehyde-PBS solution for up to 24 h. Next, they were placed in 30% sucrose solution in PBS. After the tissues were fully saturated with sucrose, they were embedded in an optimal cutting temperature compound medium (Sakura Fine Chemicals), and then frozen. Cryosections were cut using a cryostat-microtome (Leica) at 5 μm thickness. For immunofluorescence staining, frozen sections were air-dried for 30 min and then washed twice in PBS for 5 min at room temperature. Sections were then permeabilized and blocked in 2% goat serum, 1% bovine serum albumin, and 0.1% Triton X-100 in PBS at room temperature, and shaken for 1 h in a rocker (Rocker 25, Labnet International) at 20 rpm. Then the sections were incubated overnight at 4 °C with the rabbit anti-AWAT2 (NBP1–91574 from Novus Biologicals) and mouse anti-RPE65 antibody at 1:100 dilution, the sections were washed three times with PBS for 10 min and incubated with a 1:400 dilution of secondary antibody, Alexa Fluor 555 conjugated goat anti-rabbit IgG or Alexa Fluor 488 conjugated goat anti-mouse IgG (Life Technologies) in the blocking buffer. Finally, the sections were washed three times for 15 min each with PBS, mounted in a mounting medium (Prolong Gold Antifade Reagent

containing 4′,6-diamidino-2-phenylindole, Intrivogen), and covered with cover glass and allowed to dry. Fluorescent images were obtained on an Olympus FV1200 Laser Scanning Microscope using laser diode 405 nm, 50 mW for DAPI, 473 nm, 15 mW for Alexa Fluor 488, or 559 nm, 20 mW for Alexa Fluor 555 with a 20x objective on Olympus IX83 inverted microscope.

Flat-mounted retinas

For the quantification of cone photoreceptor cells, flat-mounted retinas were prepared. Enucleated eyes were fixed in 4% paraformaldyhe-PBS solution for 1 h before the retina was dissected. The dissected retinas were soaked in methanol, then fixed and flattened in 4% paraformaldyhe-PBS solution between two coverslips. Before immunostaining, flattened retinas were permeabilized in methanol, washed with PBS, and blocked in 2% goat serum in PBS containing 0.05% Tween (PBST) for 1 hour. Then, the flattened retinas were incubated overnight with shaking at 4°C with anti-S opsin (AB5407, MilliporeSigma) or anti-M opsin (AB5405, MilliporeSigma) antibody at 1:200 dilutions. The flattened retinas were washed three times with PBST for 10 min and incubated with a 1:500 dilution of secondary antibody Alexa Fluor 568 (A-11011, Thermo Fisher Scientific) for 2 h at room temperature. Finally, the retinas were washed two times for 10 min with PBST and one time with PBS, mounted with Prolong Diamond Antifade Mountant (Thermo Fisher Scientific) with the photoreceptor cell side facing the cover slip. Flat-mounted retinas were imaged on a laser scanning confocal microscope (Olympus FV1200) with a 20×/0.75-NA objective by exciting the sample with a 559 nm diode laser and collecting the emission signal at 575–620 nm. Each image consists of an 11 × 11 array of 121 tiles centered at the optic nerve, and each tile is a z-stack projection of at least 35–40 slices. The individual tiles were stitched together with the Olympus FluoView software to create the final image.

Histology and hematoxylin and eosin staining

The morphology of mouse retinas was assessed using Haemotoxylin and Eosin (H&E) staining of paraffin sections. Mouse eyes and eyelids were fixed in 4% paraformaldehyde and 1% glutaraldehyde followed by paraffin sectioning. Fixed tissues were washed with PBS and processed through a Sakura Tissue-Tek VIP E-300 vacuum infiltration paraffin processor. Briefly, tissues were placed in 70% ethanol then dehydrated by increasing concentrations of ethanol (from 70% to 100%). The ethanol was exchanged with xylene by repeated incubations for 1 h. To exchange xylene with paraffin, the samples were incubated in melted paraffin for 30 minutes. This procedure was repeated four times. The tissues were embedded in fresh paraffin using the Tissue-tek paraffin embedding center. Sections were sliced in 5 μm thickness on a Microm HM355 paraffin microtome. Paraffin sections were stained with H&E and imaged using a high resolution bright-field light microscope (Leica) connected to an Exi Aqua Blue camera (Teledyne QImaging) equipped with a 20x objective. Metamorph Imaging software (Molecular Devices).

In vivo electroretinography (ERG)

Animals were dark-adapted overnight and anesthetized with an intraperitoneal injection of a mixture of ketamine (100 mg/kg) and xylazine (20 mg/kg). Pupils were dilated with a drop of 1% atropine sulfate. Mouse body temperature was maintained at 37 °C with a heating

pad. ERG responses were measured from both eyes by contact corneal electrodes held in place by a drop of Gonak solution (Akorn). Full-field ERGs were recorded with a UTAS BigShot apparatus (LKC Technologies) using Ganzfeld-derived test flashes of calibrated green 530 nm LED light.

Rod ERG a-wave fractional flash sensitivity (S_f) was calculated from the linear part of the intensity-response curve, as follows:

$$S_f = \frac{A}{A_{max} \cdot I},$$

where A is the rod a-wave dim flash response amplitude, A_{max} is the maximal response amplitude for that eye (determined at 23.5 cd·s m^{-2}), and I is the flash strength. Similarly, M-cone ERG b-wave flash sensitivity (S_f) in mice with $Gnat1^{irdr}$ genetic background, which blocks rod signaling without affecting cone responses, was determined after normalization of the dim flash response to the maximal b-wave amplitude obtained with the brightest white light stimulus from the Xenon Flash tube (700 cd·s m^{-2}). The b-wave measurements were used for all cone *in vivo* ERG recordings because of the very small magnitude of the cone a-wave in these conditions. The sensitivity of rods or cones was first determined in the dark. To monitor the postbleach recovery of rod ERG A_{max} and rod S_f or cone S_f, the bulk (> 90%) of respective visual pigment was bleached with a 35-s exposure to 520 nm LED light focused at the surface of the cornea. The bleached pigment fraction was estimated from the following equation:

$$F = 1 - e^{(-I \cdot P \cdot t)},$$

where F is the fraction of pigment bleached, t is the duration of the light exposure (s), I is the bleaching light intensity of 520 nm LED light (1.3×10^8 photons μm^{-2} s^{-1}), and P is the photosensitivity of mouse photoreceptors at the wavelength of peak absorbance (5.7×10^{-9} μm^2 for mouse rods (35); and 7.5×10^{-9} μm^2 for mouse cones (36)). For the rest of the experiment, the mice were kept in darkness and their rod or cone sensitivity was measured periodically with a test flash. Mice were re-anesthetized every 30–40 min with a lower dose of ketamine (~1/3 of the initial dose) and a 1:1 mixture of PBS and Gonak solutions was gently applied to their eyes with a plastic syringe to protect them from drying and maintain contacts with the recording electrodes.

Ex vivo cone ERG recordings from isolated mouse retinas

Mice were dark-adapted overnight and sacrificed by CO_2 asphyxiation. The whole retina was removed from each mouse eyecup under infrared illumination and stored in oxygenated aqueous L15 (13.6 mg/ml, pH 7.4) solution (Sigma-Aldrich) containing 0.1% BSA, at room temperature. The retina was mounted on filter paper with the photoreceptor side up and placed in a perfusion chamber (37) between two electrodes connected to a differential amplifier. The tissue was perfused with Locke's solution containing 112.5 mM NaCl, 3.6 mM KCl, 2.4 mM $MgCl_2$, 1.2 mM $CaCl_2$, 10 mM HEPES, pH 7.4, 20 mM $NaHCO_3$, 3 mM Na succinate, 0.5 mM Na glutamate, 0.02 mM EDTA, and 10 mM glucose. The solution

was supplemented with 2 mM L-glutamate and 10 μM DL-2-amino-4-phosphonobutyric acid to block postsynaptic components of the photoresponse (38), and with 20 μM $BaCl_2$ to suppress the slow glial PIII component (39). The perfusion solution was continuously bubbled with a 95% O_2/5% CO_2 mixture and heated to 36–37 °C.

To isolate the cone component of the transretinal response, all experiments were performed with mice in the *Gnat1*^{irdr} genetic background. Cones in the retina were stimulated with 20-ms test flashes of calibrated 505 nm LED light. The light intensity was controlled by a computer in 0.5 log unit steps. To monitor the postbleach recovery of cone ERG a-wave flash sensitivity (S_f, see definition in a previous section), >90% of M-cone visual pigment was bleached with a 3-s exposure to 505 nm light. The bleached fraction was estimated from the same equation as described for a similar dark adaptation experiment *in vivo*:

$$F = 1 - e^{(-I \cdot P \cdot t)},$$

where F is the fraction of cone pigment bleached, t is the duration of the light exposure (in seconds), I is the bleaching light intensity of 505 nm LED light (1.6×10^8 photons μm^{-2} s^{-1}), and P is the photosensitivity of mouse cones at the wavelength of peak absorbance (7.5×10^{-9} μm^2). For the rest of the experiment, the retinas were kept in darkness and cone sensitivity was measured periodically with a test flash. Photoresponses were amplified by a differential amplifier (DP-311, Warner Instruments), low-pass filtered at 300 Hz (8-pole Bessel), and digitized at 1 kHz. Data were analyzed with Clampfit 10.4 and Origin 8.5 software.

Statistical Analyses

Unless otherwise specified, morphological and biochemical data are presented as means ± standard deviation (SD), whereas electrophysiological data are presented as means ± standard error of the mean (SEM). The number of samples and independent experiments are indicated in the figure legends. Statistical significance was assessed using one-way analysis of variance (ANOVA) followed by the Scheffe test using Origin 9 software (OriginLab Corporation). If not specified differently in the figures, thresholds of significance are set at **p<0.05, **p<0.01*, or ****p<0.001*.

RESULTS

Intra-retinal localization of AWAT2

As reported previously, the inactivation of the *Awat2* gene resulted in a phenotype characteristic of obstructive dry eye syndrome and corresponding skin abnormalities related to the blockage in wax ester production in the meibomian and sebaceous glands (30) (Fig. 1C). To verify whether AWAT2 contributes to the esterification of retinoids in the retina, we performed an AWAT2 enzymatic assay in retinal extracts obtained from WT and *Awat2*$^{-/-}$ mice. The examined WT samples revealed modest but quantifiable acyl-CoA-dependent enzymatic activity towards 11-*cis*-retinol (Fig. 1D and Supplementary Fig. 1). Interestingly, we did not observe the production of all-*trans*-retinyl esters. However, 13-*cis*-retinyl esters were readily detectable, indicating the specificity of the enzymatic activity towards *cis*-

retinols (Supplementary Fig. 1). The absence of AWAT2 led to a decline in the production of 11-*cis*-retinyl esters to the level observed for samples incubated without the acyl-CoA substrate. Thus, AWAT2 enzymatic activity contributes considerably to the biosynthesis of *cis*-retinyl esters in the mouse retinal homogenates.

Importantly, AWAT2-deficiency did not cause macroscopic developmental abnormalities within the eye, providing an opportunity to investigate the role of this enzyme in the recycling of retinal visual chromophore. For this purpose, we first examined the expression pattern of *Awat2* in the mouse retina. The immunohistochemistry of retinal sections of wildtype (WT) mice revealed a broad distribution of AWAT2 within the neural retina. The protein was detectable primarily in the photoreceptor inner segments, outer and inner plexiform layer, as well as in ganglion cells (Fig. 2A). By comparison, the immunofluorescence signal for AWAT2 was less profound in Müller cells and only partially resembled the pattern of expression characteristic for the Müller cells markers such as CRALBP (Fig. 2C) and glutamine synthetase (GluSyn) (Fig. 2D). Importantly, retinal sections isolated from *Awat2*$^{-/-}$ mice used as controls did not show any specific immunofluorescence signal, indicating the selectivity of the polyclonal antibodies (Fig. 2B). Interestingly, in addition to the retina, AWAT2 was also detectable in RPE cell layers, contradicting previously published observations (22). Therefore, we verified the expression pattern of *Awat2* in isolated retina and RPE cells by RT-PCR (Fig 2E). The signal for AWAT2 was clearly detectable in the highly purified RPE fraction, confirming the results obtained by immunohistochemistry. Therefore, AWAT2 expression is not specific to any particular cell type within the mouse retina and also includes RPE cells.

AWAT2 deficiency does not affect retinal morphology

To investigate whether AWAT2-deficiency induces any changes to the cellular structure of the retina, we examined eye sections isolated from 4-month-old mice. As indicated by the H&E staining, the morphology of *Awat2*$^{-/-}$ retinas did not reveal any abnormalities and was not distinguishable from WT counterparts of identical genetic background (Fig. 3A). Quantitative measurements of retinal morphology were provided by OCT analysis, with measurements of the thickness of ONL across the retinas indicating no difference between KO and WT groups of mice (Fig. 3B).

Cones are particularly sensitive to chromophore deficiency and degenerate in the absence of efficient chromophore supply (40–42). To examine the effect of AWAT2 deletion on cone density, WT and *Awat2*$^{-/-}$ mouse retinas were processed as flat-mounted retinas and stained against S- and M-opsins (Fig. 3C). Fluorescence intensity quantification for these two types of opsins showed no statistically significant differences in the number of cones between the experimental samples (Fig. 3D). Therefore, the absence of AWAT2 does not affect cone survival in 4-month-old mice.

AWAT2 deficiency has no detectable effect on ocular retinoid composition and regeneration of rod visual chromophore

To examine whether AWAT2 enzymatic activity contributes to the total flux of retinoids in the retina, we measured the rate of recovery of 11cRAL after ~70% of rhodopsin

photobleaching. As indicated in Fig. 4A, the average amount of 11cRAL at each examined time point after the light exposure was the same within the margin of error in *Awat2*$^{-/-}$ and WT mice. Thus, the rate of rod visual chromophore regeneration was not affected by the deletion of *Awat2* in mice. Additionally, the HPLC chromatograms indicated no detectable differences in any other retinoid metabolites such as all-*trans*-retinyl esters and all-*trans*-retinol (Fig. 4B and C). Taken together, these data support the lack of immediate impact of AWAT2 deficiency on the functional integrity of the retina or on the recycling of visual chromophore for the rods by the classic RPE visual cycle.

AWAT2 deficiency does not affect dark adaptation of rods

AWAT2 has been hypothesized to be involved in the recycling of visual chromophore in the retina (21). To begin investigating the possible functional role of AWAT2 in the mouse retina, we first examined the function of rod photoreceptors in control and *Awat2*$^{-/-}$ mice. We performed *in vivo* ERG recordings from dark-adapted control (WT) and *Awat2*$^{-/-}$ animals. The mutant mice produced robust rod-driven, scotopic, photoresponses that were comparable in waveform kinetics to these in WT mice (Fig. 5A). Interestingly, the maximal scotopic a-wave response, A_{max}, in dark-adapted (DA) *Awat2*$^{-/-}$ mice was only ~58% of that in WT mice (see DA points in Fig. 5B, C), with mean values of 281 ± 14 μV (n = 8) and 162 ± 9 μV (n = 10), respectively. Also, scotopic a-wave photosensitivity, S_f, was slightly reduced (by ~13%) in *Awat2*$^{-/-}$ (1.33 ± 0.06 m^2 cd·s^{-1}; n = 10) as compared to WT (1.54 m^2 cd·s^{-1} ± 0.07; n = 8) mice ($p < 0.05$; see also the DA points in Fig. 5D, E). There was also a proportional (~46%) reduction of the maximal rod ON bipolar cell-driven ERG b-wave response in the mutant animals (273 ± 16 μV, n = 10) as compared to WT (510 ± 36 μV; n = 8). The similar level of reduction of the scotopic a- and b-wave maximal response amplitudes suggests that the deficiency originates in the rods and is then simply propagated to the rod ON bipolar cells.

Next, to determine whether the efficiency of visual chromophore supply to rods is affected by the deletion of AWAT2, we evaluated the recovery of rod-driven a-wave ERG response following exposure of the eyes to brief bright light estimated to bleach >90% of rhodopsin. Both the scotopic maximal a-wave response amplitude (A_{max}; Fig. 5B, C) and the scotopic a-wave sensitivity (Fig. 5D, E) recovered with comparable kinetics in WT and *Awat2*$^{-/-}$ mice, confirming results obtained by retinoid analysis.

AWAT2 deficiency affects the function and dark adaptation of cones

If, as postulated, AWAT2 plays a role specifically in the chromophore recycling by retinal Muller cells, it would be expected that its deletion will selectively affect the function of cones. To address this question, we first compared the cone-driven responses from control and *Awat2*$^{-/-}$ mice in dark-adapted conditions. To isolate the cone component of the retinal total response, all mice for these cone experiments were on *Gnat1*^{irdr} background, which lacks rod function due to a mutation in rod transducin (Fig. 1B) (33). We performed transretinal recordings first, which allowed us to block pharmacologically the b-wave response and examine the sensitivity and waveform of the M-cone responses in control (*Gnat1*^{irdr}) and *Awat2*$^{-/-}$/*Gnat1*^{irdr} mice. Comparison of their dim flash responses revealed that cone responses in *Awat2*$^{-/-}$/*Gnat1*^{irdr} mice have a shape that is comparable to that

in control mice (Fig. 6A). The fractional photosensitivity was also comparable for control ($3.2\times10^{-5} \pm 2.9\times10^{-6}$ μm^2 ph^{-1}; n = 18) and *Awat2*$^{-/-}$/*Gnat1*^{irdr} ($3.7\times10^{-5} \pm 2.9\times10^{-6}$ μm^2 ph^{-1}; n = 18, $p > 0.05$) cone responses. Consistent with this, analysis of the rising phases of cone responses showed that the amplification of cone phototransduction is also not affected by the deletion of AWAT2. The saturated responses of *Awat2*$^{-/-}$/*Gnat1*^{irdr} cones also had normal kinetics, with only a slight delay in the recovery phase (Fig. 6B). Comparison of the maximal cone response amplitudes revealed that they were similar in control and mutant lines, with mean values of 23.1 ± 0.9 μV (n = 17) and 23.7 ± 1.1 μV (n = 19), respectively ($p < 0.05$). Thus, it appears that while the absence of AWAT2 suppresses the maximal rod response amplitude, it has no effect on the corresponding amplitude of the cone responses.

To further investigate the effect of AWAT2 in modulating the function of dark-adapted cones, we performed *in vivo* ERG recordings and examined the cone-driven b-wave responses. Consistent with our transretinal recordings, the dim flash cone b-wave responses of control and *Awat2*$^{-/-}$/*Gnat1*^{irdr} mice had a comparable amplitude and time to peak (Fig. 6C). Similar to our rod results, we also found that the maximal M-cone b-wave response to a bright flash was significantly reduced in *Awat2*$^{-/-}$/*Gnat1*^{irdr} mice to 63% of that in controls (Fig. 6D) with mean values of 149 ± 6 μV (n = 20) and 199 ± 17 μV (n = 18), respectively. Therefore, in contrast to rods, the absence of AWAT2 does not affect the sensitivity or maximal response of mouse M-cones and only results in a reduction in the maximal cone bipolar cell-driven response.

Finally, we examined the effect of deleting AWAT2 on the dark adaptation of M-cones. First, to isolate the function specifically of the retina visual cycle, we performed recordings from isolated retina, where the only mechanism for chromophore recycling is through the Müller cells (43). In both control and *Awat2*$^{-/-}$ retinas, exposure to a brief bright light resulted in a dramatic reduction of sensitivity caused by bleaching most of the cone visual pigment (Fig. 7A and Supplementary Fig. 2A). In darkness, this initial desensitization was followed by a rapid recovery of most of the sensitivity, so that 7 min after the bleach cone sensitivity in control retinas had recovered to ~60% of its pre-bleach dark-adapted level (Fig. 7A). A similar recovery took place in *Awat2*$^{-/-}$/*Gnat1*^{irdr} retinas (Fig. 7A), but the relative level of recovery was significantly (~23%) lower than that for control cones. The difference in recovery between control and *Awat2*$^{-/-}$/*Gnat1*^{irdr} cones can be appreciated more easily in Fig. 7B, where cone sensitivity is replotted on a linear scale. The normalized cone recovery data could be best fitted with double-exponential functions that yielded recovery time constants of 0.77 min and 9.6 min (with corresponding amplitudes of the two exponents of 0.40 and 0.25) for control and 0.82 min and 10.8 min (with corresponding exponent amplitudes of 0.33 and 0.17) for mutant mice. Thus, there was only a slight (~7%) slowing in the first rapid phase of cone sensitivity recovery after the bleach (with ~17% reduction of its estimated amplitude) in the mutant line. In contrast, the second slower phase of the recovery was compromised to a larger degree (~13%), with ~32% reduction of its estimated amplitude, in *Awat2*$^{-/-}$/*Gnat1*^{irdr} mice. While it is rather difficult to ascribe the two overlapping recovery phases to certain processes mechanistically, we believe that its first rapid component (within first 30–40 seconds after the bleach) is mostly driven by the cone phototransduction shutoff and respective recovery of the dark photovoltage, whereas the second slower phase is dominated by the regeneration of the cone visual

pigment intraretinally. Importantly, the final measured level of cone Sf recovery by 25 min post-bleach was lower by ~23% in retinas from *Awat2*$^{-/-}$/*Gnat1*^{irdr} animals (48 ± 3% vs. 62 ± 4% in controls, $p < 0.01$). This result suggests that the absence of AWAT2 partially suppresses the function of the retina visual cycle and the regeneration of cone visual pigment in the isolated retina.

To determine how AWAT2 modulates the overall dark adaptation of cones in the intact eye, we examined the dark adaptation of M-cones *in vivo* by ERG recordings. In this case, cone pigment regeneration and sensitivity recovery after a bleach are driven by the combined action of the canonical RPE visual cycle and the cone-specific retinal visual cycle. Because cone a-wave is very small and difficult to detect and measure reliably by ERG recordings *in vivo*, we used the cone b-wave as a readout of cone sensitivity. As in the transretinal recordings, the exposure to brief bright light produced a rapid decrease in sensitivity due to the bleach of most of the cone visual pigments (Fig. 7C and Supplementary Fig. 2B). In control mice, the cone ERG b-wave sensitivity then recovered in two phases, a rapid phase over the first 10 min, driven by the retina visual cycle, and a second slow phase over the next 50 min, driven by the canonical RPE visual cycle (43). As a result, 60 min after the bleach cone b-wave sensitivity had recovered to 85% of its pre-bleach level (Fig. 7C). In *Awat2*$^{-/-}$/*Gnat1*^{irdr} mice, the cone b-wave also recovered robustly (Fig. 7C), but both the initial rapid phase and the second slower phase of cone recovery were significantly suppressed compared to controls. The difference in recovery between control and *Awat2*$^{-/-}$ mice can be appreciated more easily in Fig. 7D, where cone b-wave sensitivity is replotted on a linear scale. It should be noted that the very initial rapid component of the recovery (corresponding to the first recovery phase observed *ex vivo*) was not largely visible in these cone ERG b-wave recordings, likely due to the longer bleaching step used in these conditions as well as several seconds-long technical delay in the measurement at the first post-bleach time point. Together, these results clearly demonstrate that the absence of AWAT2 suppresses the regeneration of M-cone visual pigment by affecting the recycling of chromophore by both the cone-specific retina and the canonical RPE visual cycle.

DISCUSSION

Gene screening methodology has been successfully applied to identify RPE65 as a functional retinoid isomerase in RPE cells, bringing an end to the decades long quest for an 11-*cis*-retinol (11cROL)-producing enzyme (44). The implementation of the same experimental approach to search for proteins involved in the cone-specific regeneration pathway led to the identification of two gene candidates, *Des1* and *Awat2* (21, 22). Based on biochemical analysis, the protein products of these two genes were believed to work cooperatively, enabling the formation of a readily accessible pool of 11-*cis* retinoids for cone pigment regeneration. In this model, DES1 catalyzes the rapid isomerization of atROL yielding an equilibrium mixture of *cis* isomers, whereas AWAT2 removes 11cROL from the mixture by its selective esterification (22). However, unlike RPE65, the enzymatic activity of which was confirmed by prior genetic evidence of the lack of visual chromophore in *Rpe65*$^{-/-}$ mice (45), the physiological role of DES1 and AWAT2 in the regeneration of cone pigment remained to be investigated. Subsequently, an independent examination of Müller cell-specific *Des1* knockout mice revealed the absence of a measurable effect on

retinal morphology or the detectable impairment of cone functions (25). In addition, the pharmacological treatment of cone-dominant ground squirrels with fenretinide, an inhibitor of DES1 activity (46), did not result in delayed cone dark adaptation kinetics (16).

Although somewhat disappointing, the above findings do not exclude the possibility that AWAT2 serves a distinct role in retinal physiology as previously proposed (22). Aside from robust wax ester formation and its role in tear film lipid biosynthesis (30, 47), the preferential substrate specificity of AWAT2 towards *cis* ROLs may indicate a DES1-independent and tissue-specific function of the enzyme in retinoid metabolism (22, 29). Therefore, we looked for a potential retina-related phenotype of *Awat2*$^{-/-}$ mice. Our analysis indicated that the dry eye syndrome related to loss of AWAT2 activity is not accompanied by morphological abnormalities within the mouse retina. Moreover, we did not observe any detectable anomalies in the canonical visual cycle retinoid metabolism or rod function. Because in rod-dominant animals standard analytical techniques do not allow for the reliable quantification of changes in retinoid composition related to cone functions, we generated *Awat2*$^{-/-}$ mice on the *Gnat1*^{irdr} mutation genetic background. By recording the M-cone-specific ERG responses in both *ex* and *in vivo* experimental settings, we were able to demonstrate that AWAT2 activity is required for the rapid cone dark adaptation. Altogether, our electrophysiological data are consistent with a biological role of AWAT2 in modulating the efficient regeneration of visual pigment in mouse cone photoreceptors. Our data also revealed significant suppression of the rod responses but not cone responses in AWAT2-deficient retinas. Considering the lack of detectable retinal degeneration (Fig. 3), these findings suggest that AWAT2 might also be required for maintaining the optimal lipid composition to support robust light responses in rod photoreceptors. Finally, we also observed a suppression of the cone-driven b-wave that, unlike the case in rods, was not associated with a reduction in the cone response in mice lacking AWAT2. This indicates a direct effect of AWAT2-deficiency on the signal propagation from cones to cone ON bipolar cells. This is in contrast to the proportional reduction in scotopic a-wave and b-wave responses observed in AWAT2-deficient mice, which indicates no intrinsic deficiency in the signal propagation from rods to rod ON bipolar cells. While the reason for this surprising difference between rods and cones is unclear at the moment, it most likely indicates a distinct role for AWAT2 in defining the lipid milieu in rod and cone photoreceptors and their respective ON bipolar cells.

AWAT2's contribution to biological processes seems to depend on cell types and available substrates. AWAT2 activity towards monounsaturated long chain alcohols is several fold higher as compared to their saturated counterparts (28). The presence of a double bond in the *Z* configuration introduces a bend or 'kink' in the structure of an aliphatic chain of the alcohol substrates that mimics the structure of *cis* retinoids. Thus, the preferential esterification of *cis* retinols as compared to atROL seems to reflect general properties of the enzyme. Nevertheless, an obvious limitation of this study is that it was performed on rod-dominant mice, restraining the use of analytical methods to follow the cone-specific flux of retinoids. Thus, it remains unclear whether the absence of AWAT2-catalyzed biosynthesis of 11-*cis*-retinyl esters is fully responsible for the observed cone phenotype. In fact, we cannot exclude the possibility that the observed delay of cone dark-adaptation in *Awat2*$^{-/-}$ mice may be related to subtle changes in the content or composition of lipids other than

retinyl esters. The absence of the *Awat2* gene orthologue in zebrafish may suggest the lack of a decisive role for this enzyme in the 11-*cis*-retinyl ester accumulation characteristic for cone-dominant retinas (48, 49). Mono-, di-, and triacylglycerols are natural components of photoreceptor outer segments (50). Particularly, polyunsaturated diacylglycerols (DAGs) reveal important biological activity by serving as secondary messengers and altering the physicochemical properties of the lipid membranes (51, 52). Thus, potential imbalance in DAGs homeostasis caused by the absence of AWAT2 activity may have an indirect effect on phototransduction, neurotransmission or intracellular transport of retinoids (53, 54). Consistent with this, we observed significant reduction in the maximal response of rods even though their dark adaptation and chromophore supply through the canonical RPE-dependent visual cycle remained normal.

Although our results demonstrate a role of AWAT2 in retinal physiology, the question about alternative mechanisms supporting the cone-specific regeneration of visual pigments remains. Unlike rods, cones can operate in bright light conditions. Therefore, the re-isomerization of cone visual chromophore could be driven by the abundant source of energy provided by incoming photons, yielding a fast and light intensity-dependent reisomerization of atRAL. Two mechanisms have been proposed that may contribute to the photic production of visual chromophore: nonenzymatic conversion of atRAL via a phospholipid intermediate (55, 56) and retinal G protein-coupled receptor (RGR)-mediated generation of 11cRAL (57–59). In the first process, the formation of a Schiff base between atRAL and phosphatidylethanolamine (PE) in the photoreceptor's outer segment membranes increases the quantum efficiency of blue light (450 nm)-dependent photoisomerization of the N-ret-PE conjugate. In contrast, RGR opsin isomerization occurs at longer wavelength (505–535 nm) (59). Because of the single step quantum reaction catalyzed by RGR, the activity of this receptor can make a significant contribution to the readily available pool of 11cRAL in RPE and Müller cells. Although appealing, both mechanisms have not been fully integrated into the canonical visual cycle and seem not to be autonomous pathways for 11cRAL supplementation as neither of them provides a sufficient amount of the visual chromophore to sustain cone functions in the absence of RPE65. Also, they do not explain the robust accumulation of 11-*cis*-retinyl esters in the retina and RPE cell of cone-dominant species – an observation consistent with a role for AWAT2 in chromophore production in these species. Lastly, the proposed mechanisms focus on the mechanistic aspect of isomerization and ignore the transport of retinoids between the adjacent RPE, Müller, and photoreceptor cells that constitutes an important element of regeneration kinetics. Answering these and other questions related to cone physiology will require the development of genetically modified cone-rich animal models that will alleviate the current limitations of mouse lines.

Supplementary Material

Refer to Web version on PubMed Central for supplementary material.

ACKNOWLEGMENTS

We thank Catherine Doller, Anthony Gardella, and Maryanne Pendergast from the Visual Science Core Facility at CWRU for their expert help with histology, microscopy, and imaging. Also, we would like to acknowledge Wiktor Golczak for his contribution to the editing of this manuscript. This work was supported by NIH grants EY023948

(M.G.), EY025696 and EY030912 (V.J.K.), and NIH P30 core grant EY011373 to the Visual Sciences Research Center Core Facilities at CWRU, and an unrestricted grant from Research to Prevent Blindness to the Department of Ophthalmology at the University of California Irvine.

DATA AVAILABILITY STATMENT

The data that support the findings of this study as well as information about the equipment and software used to process the data are available in the methods section and/or supplementary material of this article.

ABBREVIATIONS

11cRAL	11-*cis*-retinal
AWAT2	acyl-CoA wax alcohol acyltransferase 2
CRALBP	cellular retinaldehyde-binding protein
DAGs	diacylglycerols
ERG	electroretinography
Gnat1	rod transducin α-subunit
GluSyn	glutamine synthetase
H&E	Haemotoxylin and Eosin staining
LC-MS	liquid chromatography mass spectrometry
LRAT	lecithin:retinol acyltransferase
MFAT	multifunctional *O*-acyltransferase
RPE	retinal pigment epithelium
RPE65	retinal pigment epithelium-specific 65 kDa protein
SD-OCT	spectral domain optical coherence tomography
WT	wild type

References:

1. Ingram NT, Sampath AP, and Fain GL (2016) Why are rods more sensitive than cones? J Physiol 594, 5415–5426 [PubMed: 27218707]
2. Molday RS, and Moritz OL (2015) Photoreceptors at a glance. J Cell Sci 128, 4039–4045 [PubMed: 26574505]
3. Luo DG, Xue T, and Yau KW (2008) How vision begins: an odyssey. Proc Natl Acad Sci U S A 105, 9855–9862 [PubMed: 18632568]
4. Hofmann L, and Palczewski K (2015) Advances in understanding the molecular basis of the first steps in color vision. Prog Retin Eye Res 49, 46–66 [PubMed: 26187035]
5. Kefalov VJ (2012) Rod and cone visual pigments and phototransduction through pharmacological, genetic, and physiological approaches. J Biol Chem 287, 1635–1641 [PubMed: 22074928]

6. Kefalov V, Fu Y, Marsh-Armstrong N, and Yau KW (2003) Role of visual pigment properties in rod and cone phototransduction. Nature 425, 526–531 [PubMed: 14523449]
7. Nathans J (1999) The evolution and physiology of human color vision: insights from molecular genetic studies of visual pigments. Neuron 24, 299–312 [PubMed: 10571225]
8. Hofmann KP, Scheerer P, Hildebrand PW, Choe HW, Park JH, Heck M, and Ernst OP (2009) A G protein-coupled receptor at work: the rhodopsin model. Trends Biochem Sci 34, 540–552 [PubMed: 19836958]
9. Kiser PD, Golczak M, and Palczewski K (2014) Chemistry of the retinoid (visual) cycle. Chemical reviews 114, 194–232 [PubMed: 23905688]
10. Kiser PD, Zhang J, Badiee M, Li Q, Shi W, Sui X, Golczak M, Tochtrop GP, and Palczewski K (2015) Catalytic mechanism of a retinoid isomerase essential for vertebrate vision. Nat Chem Biol 11, 409–415 [PubMed: 25894083]
11. Golczak M, Sears AE, Kiser PD, and Palczewski K (2015) LRAT-specific domain facilitates vitamin A metabolism by domain swapping in HRASLS3. Nat Chem Biol 11, 26–32 [PubMed: 25383759]
12. Redmond TM, Yu S, Lee E, Bok D, Hamasaki D, Chen N, Goletz P, Ma JX, Crouch RK, and Pfeifer K (1998) Rpe65 is necessary for production of 11-cis-vitamin A in the retinal visual cycle. Nat Genet 20, 344–351 [PubMed: 9843205]
13. Batten ML, Imanishi Y, Maeda T, Tu DC, Moise AR, Bronson D, Possin D, Van Gelder RN, Baehr W, and Palczewski K (2004) Lecithin-retinol acyltransferase is essential for accumulation of all-trans-retinyl esters in the eye and in the liver. J Biol Chem 279, 10422–10432 [PubMed: 14684738]
14. Jacobson SG, Aleman TS, Cideciyan AV, Heon E, Golczak M, Beltran WA, Sumaroka A, Schwartz SB, Roman AJ, Windsor EA, Wilson JM, Aguirre GD, Stone EM, and Palczewski K (2007) Human cone photoreceptor dependence on RPE65 isomerase. Proc Natl Acad Sci U S A 104, 15123–15128 [PubMed: 17848510]
15. Fan J, Rohrer B, Moiseyev G, Ma JX, and Crouch RK (2003) Isorhodopsin rather than rhodopsin mediates rod function in RPE65 knock-out mice. Proc Natl Acad Sci U S A 100, 13662–13667 [PubMed: 14578454]
16. Kiser PD, Zhang J, Sharma A, Angueyra JM, Kolesnikov AV, Badiee M, Tochtrop GP, Kinoshita J, Peachey NS, Li W, Kefalov VJ, and Palczewski K (2018) Retinoid isomerase inhibitors impair but do not block mammalian cone photoreceptor function. J Gen Physiol 150, 571–590 [PubMed: 29500274]
17. Mahroo OA, and Lamb TD (2004) Recovery of the human photopic electroretinogram after bleaching exposures: estimation of pigment regeneration kinetics. J Physiol 554, 417–437 [PubMed: 14594984]
18. Mata NL, Radu RA, Clemmons RC, and Travis GH (2002) Isomerization and oxidation of vitamin a in cone-dominant retinas: a novel pathway for visual-pigment regeneration in daylight. Neuron 36, 69–80 [PubMed: 12367507]
19. Xue Y, Shen SQ, Jui J, Rupp AC, Byrne LC, Hattar S, Flannery JG, Corbo JC, and Kefalov VJ (2015) CRALBP supports the mammalian retinal visual cycle and cone vision. J Clin Invest 125, 727–738 [PubMed: 25607845]
20. Lima de Carvalho JR Jr., Kim HJ, Ueda K, Zhao J, Owji AP, Yang T, Tsang SH, and Sparrow JR (2020) Effects of deficiency in the RLBP1-encoded visual cycle protein CRALBP on visual dysfunction in humans and mice. J Biol Chem 295, 6767–6780 [PubMed: 32188692]
21. Kaylor JJ, Yuan Q, Cook J, Sarfare S, Makshanoff J, Miu A, Kim A, Kim P, Habib S, Roybal CN, Xu T, Nusinowitz S, and Travis GH (2013) Identification of DES1 as a vitamin A isomerase in Muller glial cells of the retina. Nature chemical biology 9, 30–36 [PubMed: 23143414]
22. Kaylor JJ, Cook JD, Makshanoff J, Bischoff N, Yong J, and Travis GH (2014) Identification of the 11-cis-specific retinyl-ester synthase in retinal Muller cells as multifunctional O-acyltransferase (MFAT). Proc Natl Acad Sci U S A 111, 7302–7307 [PubMed: 24799687]
23. Ternes P, Franke S, Zahringer U, Sperling P, and Heinz E (2002) Identification and characterization of a sphingolipid delta 4-desaturase family. J Biol Chem 277, 25512–25518 [PubMed: 11937514]

24. Yen CL, Brown C. H. t., Monetti M, and Farese RV Jr. (2005) A human skin multifunctional O-acyltransferase that catalyzes the synthesis of acylglycerols, waxes, and retinyl esters. J Lipid Res 46, 2388–2397 [PubMed: 16106050]
25. Kiser PD, Kolesnikov AV, Kiser JZ, Dong Z, Chaurasia B, Wang L, Summers SA, Hoang T, Blackshaw S, Peachey NS, Kefalov VJ, and Palczewski K (2019) Conditional deletion of Des1 in the mouse retina does not impair the visual cycle in cones. FASEB J 33, 5782–5792 [PubMed: 30645148]
26. Ward R, Kaylor JJ, Cobice DF, Pepe DA, McGarrigle EM, Brockerhoff SE, Hurley JB, Travis GH, and Kennedy BN (2020) Non-photopic and photopic visual cycles differentially regulate immediate, early, and late phases of cone photoreceptor-mediated vision. J Biol Chem 295, 6482–6497 [PubMed: 32238432]
27. Turkish AR, Henneberry AL, Cromley D, Padamsee M, Oelkers P, Bazzi H, Christiano AM, Billheimer JT, and Sturley SL (2005) Identification of two novel human acyl-CoA wax alcohol acyltransferases: members of the diacylglycerol acyltransferase 2 (DGAT2) gene superfamily. J Biol Chem 280, 14755–14764 [PubMed: 15671038]
28. Miklaszewska M, Kawinski A, and Banas A (2013) Detailed characterization of the substrate specificity of mouse wax synthase. Acta Biochim Pol 60, 209–215 [PubMed: 23730681]
29. Arne JM, Widjaja-Adhi MA, Hughes T, Huynh KW, Silvaroli JA, Chelstowska S, Moiseenkova-Bell VY, and Golczak M (2017) Allosteric modulation of the substrate specificity of acyl-CoA wax alcohol acyltransferase 2. J Lipid Res 58, 719–730 [PubMed: 28096191]
30. Widjaja-Adhi MAK, Silvaroli JA, Chelstowska S, Trischman T, Bederman I, Sayegh R, and Golczak M (2020) Deficiency in Acyl-CoA:Wax Alcohol Acyltransferase 2 causes evaporative dry eye disease by abolishing biosynthesis of wax esters. FASEB J 34, 13792–13808 [PubMed: 32851726]
31. Vincent SD, and Robertson EJ (2003) Highly efficient transgene-independent recombination directed by a maternally derived SOX2CRE transgene. Genesis 37, 54–56 [PubMed: 14595840]
32. Hayashi S, Tenzen T, and McMahon AP (2003) Maternal inheritance of Cre activity in a Sox2Cre deleter strain. Genesis 37, 51–53 [PubMed: 14595839]
33. Deng WT, Sakurai K, Liu J, Dinculescu A, Li J, Pang J, Min SH, Chiodo VA, Boye SL, Chang B, Kefalov VJ, and Hauswirth WW (2009) Functional interchangeability of rod and cone transducin alpha-subunits. Proc Natl Acad Sci U S A 106, 17681–17686 [PubMed: 19815523]
34. Golczak M, Bereta G, Maeda A, and Palczewski K (2010) Molecular biology and analytical chemistry methods used to probe the retinoid cycle. Methods Mol Biol 652, 229–245 [PubMed: 20552432]
35. Woodruff ML, Lem J, and Fain GL (2004) Early receptor current of wild-type and transducin knockout mice: photosensitivity and light-induced Ca2+ release. J Physiol 557, 821–828 [PubMed: 15073279]
36. Nikonov SS, Kholodenko R, Lem J, and Pugh EN Jr. (2006) Physiological features of the S- and M-cone photoreceptors of wild-type mice from single-cell recordings. J Gen Physiol 127, 359–374 [PubMed: 16567464]
37. Vinberg F, Kolesnikov AV, and Kefalov VJ (2014) Ex vivo ERG analysis of photoreceptors using an in vivo ERG system. Vision Res 101, 108–117 [PubMed: 24959652]
38. Sillman AJ, Ito H, and Tomita T (1969) Studies on the mass receptor potential of the isolated frog retina. I. General properties of the response. Vision Res 9, 1435–1442 [PubMed: 5367433]
39. Nymark S, Heikkinen H, Haldin C, Donner K, and Koskelainen A (2005) Light responses and light adaptation in rat retinal rods at different temperatures. J Physiol 567, 923–938 [PubMed: 16037091]
40. Rohrer B, Lohr HR, Humphries P, Redmond TM, Seeliger MW, and Crouch RK (2005) Cone opsin mislocalization in Rpe65−/− mice: a defect that can be corrected by 11-cis retinal. Invest Ophthalmol Vis Sci 46, 3876–3882 [PubMed: 16186377]
41. Parker RO, Fan J, Nickerson JM, Liou GI, and Crouch RK (2009) Normal cone function requires the interphotoreceptor retinoid binding protein. J Neurosci 29, 4616–4621 [PubMed: 19357286]

42. Jin M, Li S, Nusinowitz S, Lloyd M, Hu J, Radu RA, Bok D, and Travis GH (2009) The role of interphotoreceptor retinoid-binding protein on the translocation of visual retinoids and function of cone photoreceptors. J Neurosci 29, 1486–1495 [PubMed: 19193895]
43. Kolesnikov AV, Tang PH, Parker RO, Crouch RK, and Kefalov VJ (2011) The mammalian cone visual cycle promotes rapid M/L-cone pigment regeneration independently of the interphotoreceptor retinoid-binding protein. J Neurosci 31, 7900–7909 [PubMed: 21613504]
44. Jin M, Li S, Moghrabi WN, Sun H, and Travis GH (2005) Rpe65 is the retinoid isomerase in bovine retinal pigment epithelium. Cell 122, 449–459 [PubMed: 16096063]
45. Ma JX, Zhang D, Laser M, Brownlee NA, Re GG, Hazen-Martin DJ, Redmond TM, and Crouch RK (1999) Identification of RPE65 in transformed kidney cells. FEBS Lett 452, 199–204 [PubMed: 10386590]
46. Holland WL, Brozinick JT, Wang LP, Hawkins ED, Sargent KM, Liu Y, Narra K, Hoehn KL, Knotts TA, Siesky A, Nelson DH, Karathanasis SK, Fontenot GK, Birnbaum MJ, and Summers SA (2007) Inhibition of ceramide synthesis ameliorates glucocorticoid-, saturated-fat-, and obesity-induced insulin resistance. Cell Metab 5, 167–179 [PubMed: 17339025]
47. Sawai M, Watanabe K, Tanaka K, Kinoshita W, Otsuka K, Miyamoto M, Sassa T, and Kihara A (2021) Diverse meibum lipids produced by Awat1 and Awat2 are important for stabilizing tear film and protecting the ocular surface. iScience 24, 102478 [PubMed: 34113821]
48. Holmes RS (2010) Comparative genomics and proteomics of vertebrate diacylglycerol acyltransferase (DGAT), acyl CoA wax alcohol acyltransferase (AWAT) and monoacylglycerol acyltransferase (MGAT). Comp Biochem Physiol Part D Genomics Proteomics 5, 45–54 [PubMed: 20374941]
49. Babino D, Perkins BD, Kindermann A, Oberhauser V, and von Lintig J (2015) The role of 11-cis-retinyl esters in vertebrate cone vision. FASEB J 29, 216–226 [PubMed: 25326538]
50. Sander CL, Sears AE, Pinto AFM, Choi EH, Kahremany S, Gao F, Salom D, Jin H, Pardon E, Suh S, Dong Z, Steyaert J, Saghatelian A, Skowronska-Krawczyk D, Kiser PD, and Palczewski K (2021) Nano-scale resolution of native retinal rod disk membranes reveals differences in lipid composition. J Cell Biol 220
51. Carrasco S, and Merida I (2007) Diacylglycerol, when simplicity becomes complex. Trends Biochem Sci 32, 27–36 [PubMed: 17157506]
52. Campomanes P, Zoni V, and Vanni S (2019) Local accumulation of diacylglycerol alters membrane properties nonlinearly due to its transbilayer activity. Commun Chem 2, 72.
53. Goni FM, and Alonso A (1999) Structure and functional properties of diacylglycerols in membranes. Prog Lipid Res 38, 1–48 [PubMed: 10396601]
54. Giusto NM, Pasquare SJ, Salvador GA, and Ilincheta de Boschero MG (2010) Lipid second messengers and related enzymes in vertebrate rod outer segments. J Lipid Res 51, 685–700 [PubMed: 19828910]
55. Groenendijk GW, Jacobs CW, Bonting SL, and Daemen FJ (1980) Dark isomerization of retinals in the presence of phosphatidylethanolamine. Eur J Biochem 106, 119–128 [PubMed: 7341223]
56. Kaylor JJ, Xu T, Ingram NT, Tsan A, Hakobyan H, Fain GL, and Travis GH (2017) Blue light regenerates functional visual pigments in mammals through a retinyl-phospholipid intermediate. Nat Commun 8, 16 [PubMed: 28473692]
57. Chen P, Hao W, Rife L, Wang XP, Shen D, Chen J, Ogden T, Van Boemel GB, Wu L, Yang M, and Fong HK (2001) A photic visual cycle of rhodopsin regeneration is dependent on Rgr. Nat Genet 28, 256–260 [PubMed: 11431696]
58. Morshedian A, Kaylor JJ, Ng SY, Tsan A, Frederiksen R, Xu T, Yuan L, Sampath AP, Radu RA, Fain GL, and Travis GH (2019) Light-Driven Regeneration of Cone Visual Pigments through a Mechanism Involving RGR Opsin in Muller Glial Cells. Neuron 102, 1172–1183 e1175 [PubMed: 31056353]
59. Zhang J, Choi EH, Tworak A, Salom D, Leinonen H, Sander CL, Hoang TV, Handa JT, Blackshaw S, Palczewska G, Kiser PD, and Palczewski K (2019) Photic generation of 11-cis-retinal in bovine retinal pigment epithelium. J Biol Chem 294, 19137–19154 [PubMed: 31694912]

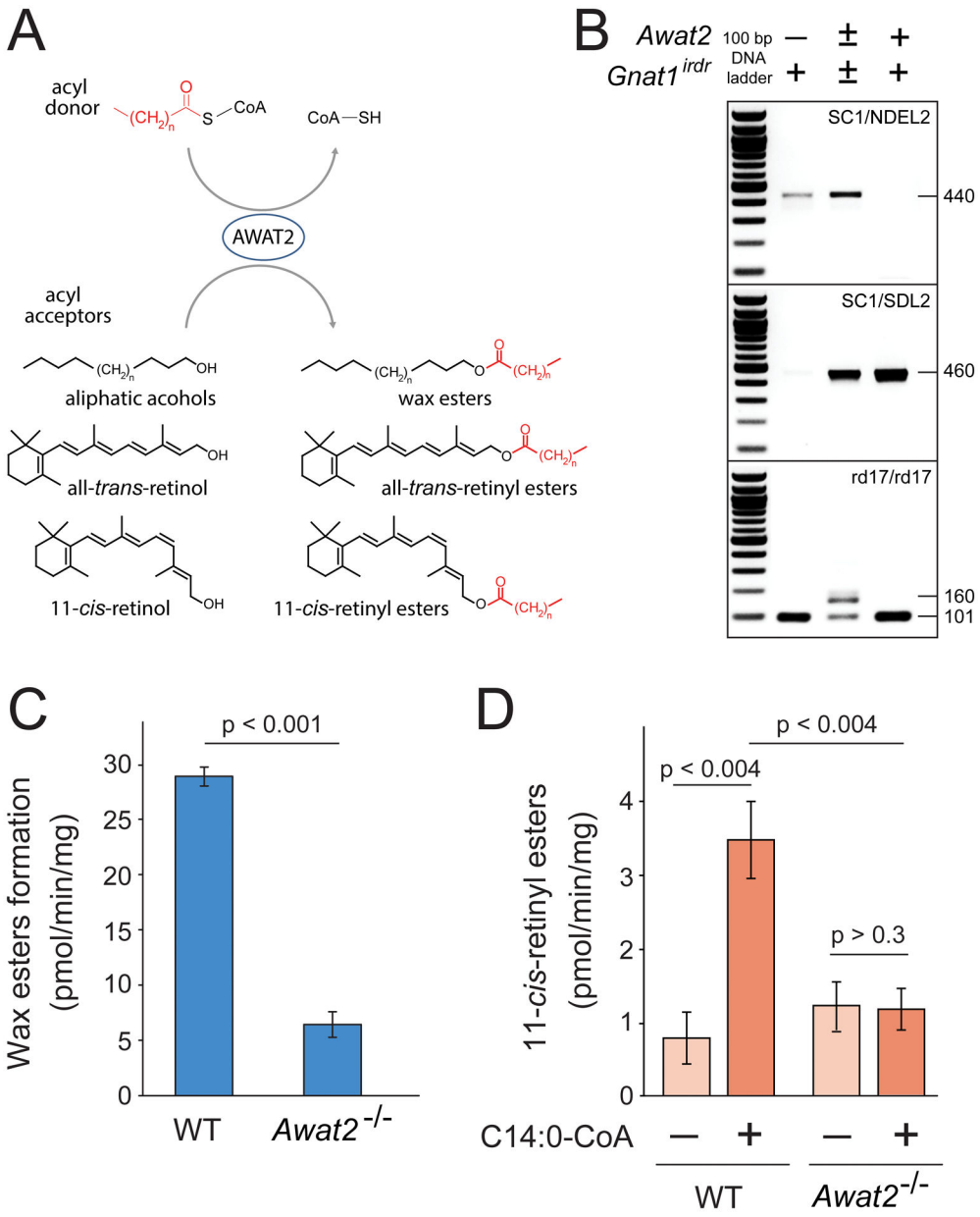

Figure 1 –. *O*-acyltransferase activity of AWAT2 in WT and *Awat2*$^{-/-}$ mice.

A, schematic representation of *O*-acyltransferase activity of AWAT2 towards lipid substrates. **B**, gel images of genomic PCR products used to detect deletion of the *Awat2* gene and mutations in the *Gnat1* gene. The bottom gel demonstrates the presence of *Gnat1*^{irdr} mutation in the mice used in this study (101 bp band indicates the presence of mutation rd17/rd17; 160 bp represent a wild type). **C**, *O*-acyltransferase assay conducted by using epidermis lysates as the source of enzymatic activity. The absence of AWAT2 dramatically diminishes acyl-CoA-dependent synthesis of myristyl myristate (wax ester). **D**, Acyl-CoA-dependent esterification of 11-*cis*-retinol in retinal homogenates from WT and *Awat2*$^{-/-}$ mice. The absence of AWAT2 activity leads to decline of the production of 11-*cis*-retinyl myristate to the level observed in control samples lacking C14:0-CoA. Enzymatic activity

data are presented as mean specific activity ± SD (standard deviation) for 4 to 6 biological replicates in each group.

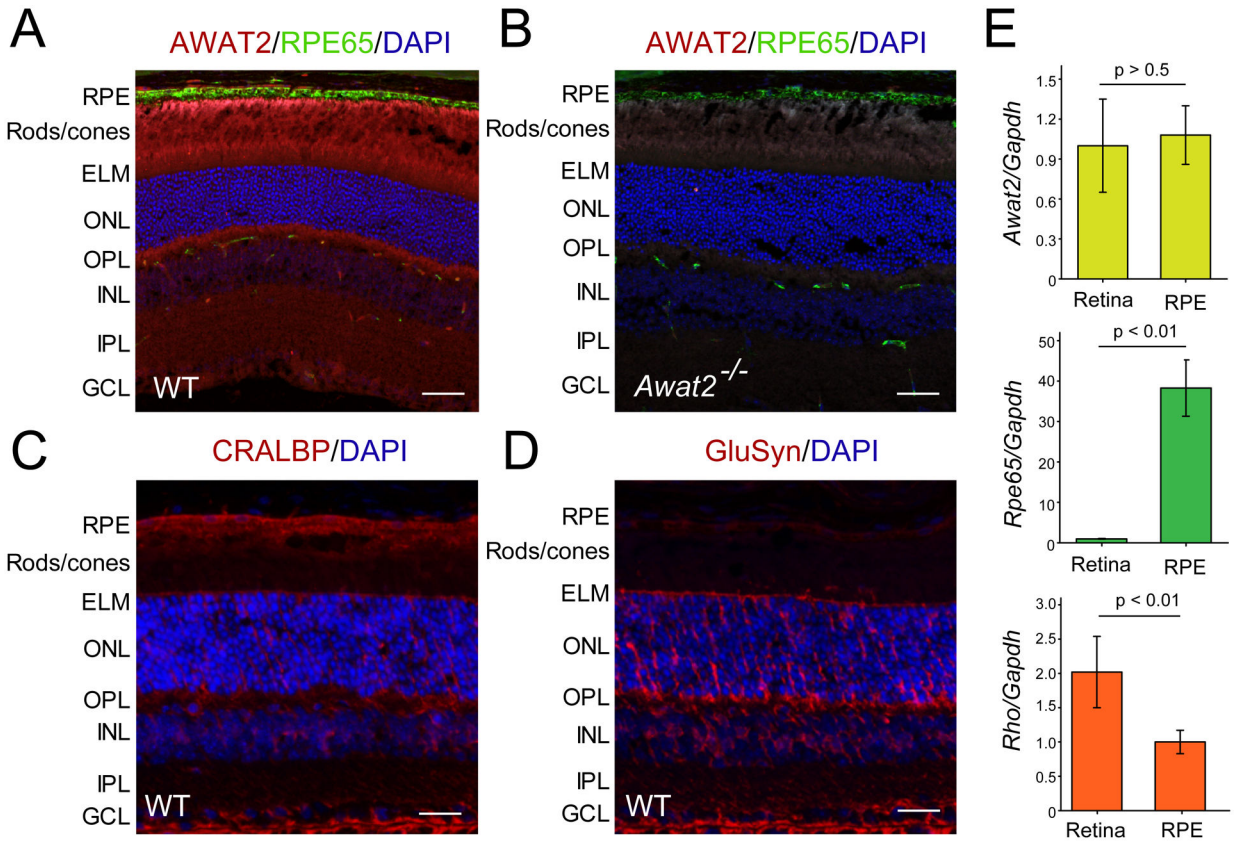

Figure 2 –. Localization of AWAT2 within the mouse retina.

A, immunofluorescence staining of mouse retina with anti-AWAT2 antibody (red), anti-RPE65 antibody (green), and DAPI (blue). Specificity of the immunostaining was verified in retinas isolated from *Awat2*$^{-/-}$ mice (**B**). For comparison, bottom images represent localization of CRALBP (expressed in RPE and Müller cells), and glutamine synthetase (GluSyn), expressed exclusively in Müller cells (panels **C** and **D**, respectively). Expression of AWAT2 was detectable primarily in the photoreceptor inner segments, outer and inner plexiform layer with less profound presence in Müller cells. Scale bars correspond to 50 μm. **E**, distribution of *Awat2* mRNA between mouse retina and RPE cells indicates that AWAT2 expression is not limited to the retinal cells, but also includes RPE. The quality of cell separation was verified by assessing mRNA levels of *Rpe65* and *Rho*.

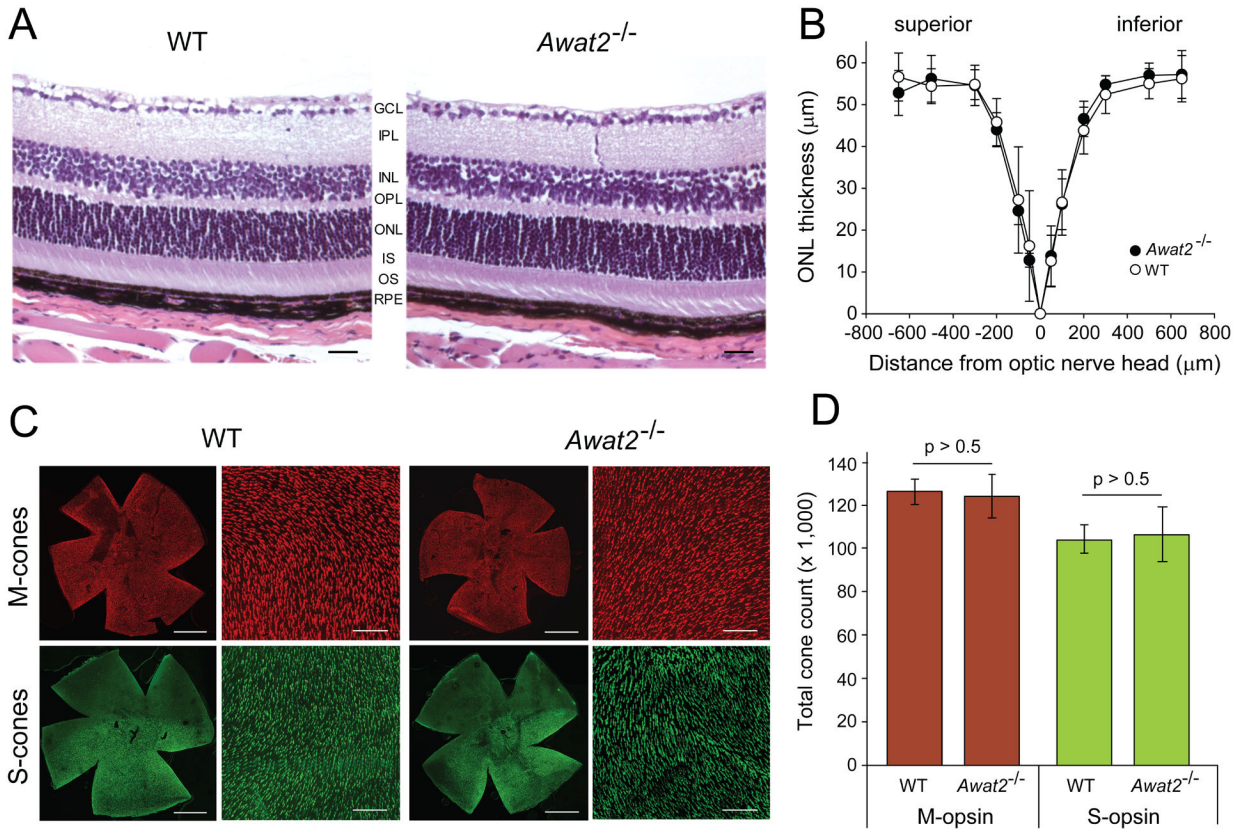

Figure 3 –. The absence of functional AWAT2 does not cause retinal degeneration.

A, morphology of WT and *Awat2*$^{-/-}$ retinas from 3- to 4-month-old mice kept under ambient room light conditions. RPE, retinal pigmented epithelium; OS, outer segment; IS, inner segment; ONL, outer nuclear layer; OPL, outer plexiform layer; INL, inner nuclear layer; IPL, inner plexiform layer; GCL, ganglion cell. Scale bar corresponds to 50 μm. **B**, photoreceptor thickness quantified by OCT plotted for WT and *Awat2*$^{-/-}$ mice. No differences in the retinal morphology were observed in any other experimental groups (n = 6). **C**, representative images of immunodetection of M- and S-cones in flat-mounted retinas. The retinas were obtained from 3- to 4-month-old WT and *Awat2*$^{-/-}$ mice. Bars correspond to 1 mm in the whole mounts and 0.4 mm in higher magnification pictures. **D**, quantification of the total number of cones in examined retinas. Six images were taken from six different mice per experimental group. Data show average ± SD. No significant differences were detected between WT and *Awat2*$^{-/-}$ mice as indicated by $p > 0.5$.

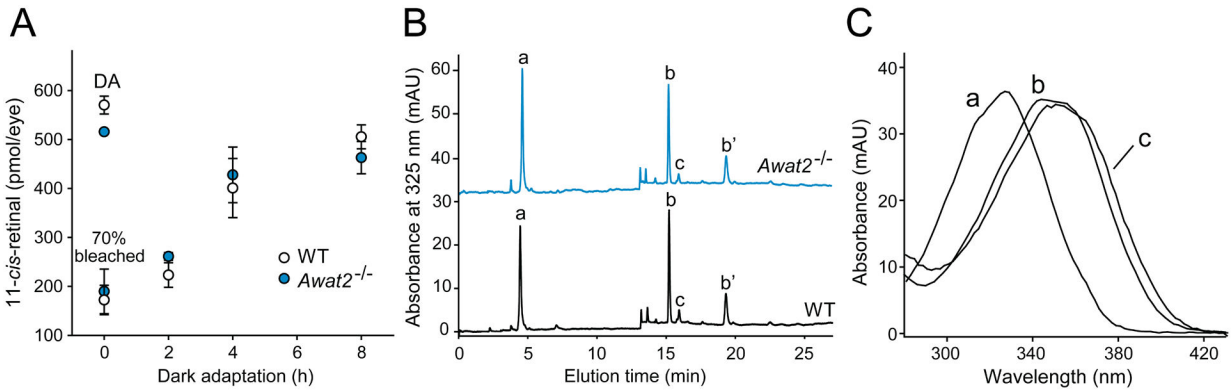

Figure 4 –. AWAT2 deletion does not affect the canonical RPE visual cycle.

A, the rate of visual chromophore regeneration after exposure to bright light. Graph represents the recovery of 11-*cis*-retinal as a function of time after photobleaching of WT and AWAT2-deficient mice. Each experimental point corresponds to an average value obtained from six eye samples. Error bars represent SD. **B**, representative chromatogram of retinoid species identified in the eye extracts of examined mice. Peak [a] represents all-*trans*-retinyl esters, peaks [b] and [b'] – 11-*cis*-retinal *syn* and *anti*-forms, respectively, whereas peak [c] corresponds to all-*trans*-retinal. **C**, UV/Vis spectra for the corresponding chromatography peaks found in chromatograms shown in panel B.

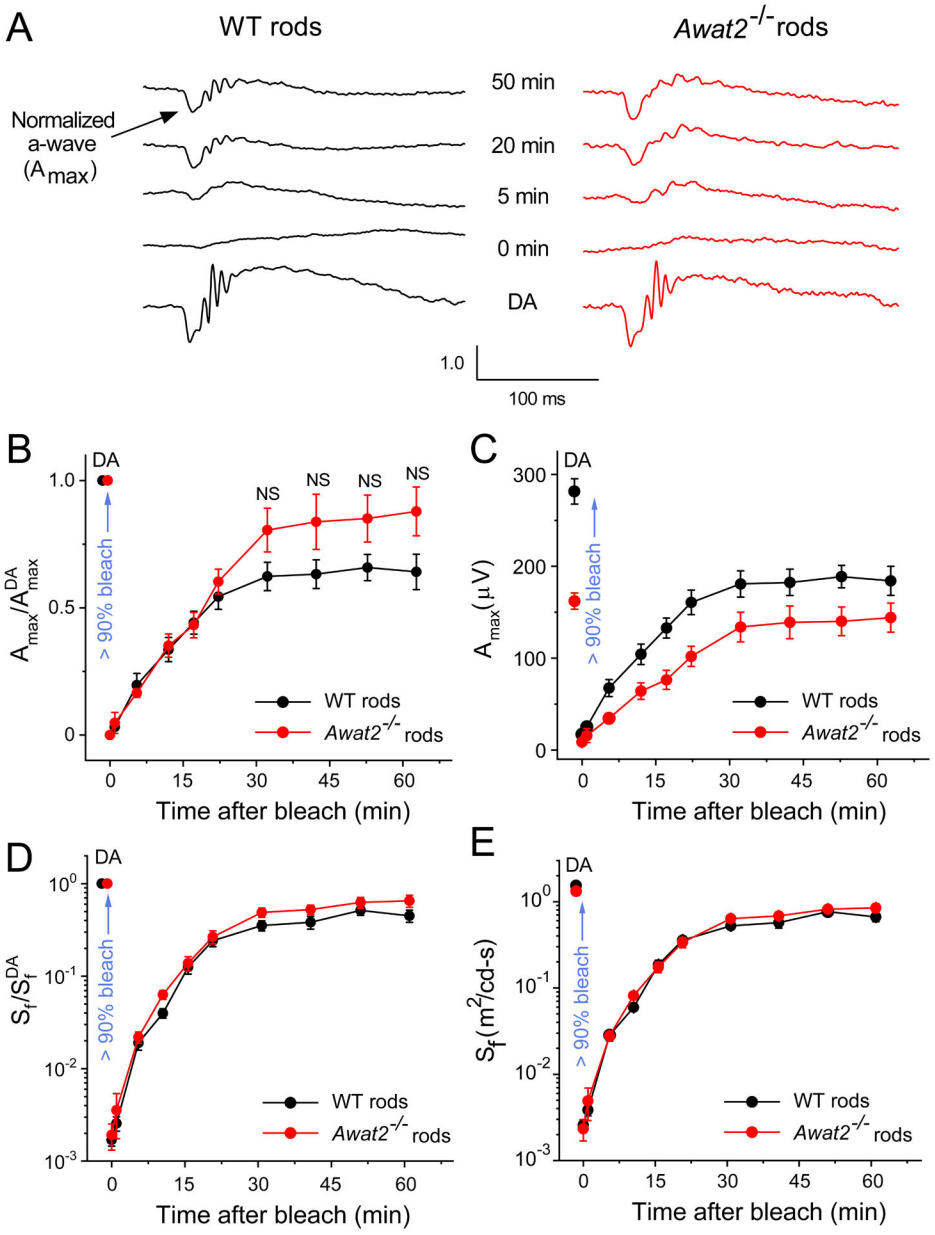

Figure 5 –. Normal rod dark adaptation in AWAT2-deficient mice.

A, representative scotopic ERG responses in the dark (dark-adapted [DA], bottom) and at four indicated time points after bleaching > 90% of the rod pigment in WT (left) and *Awat2*$^{-/-}$ (right) mice. For each time point, A_{max} values were normalized to their corresponding pre-bleach dark-adapted value (A_{max}^{DA}). **B**, recovery of normalized scotopic ERG maximal a-wave amplitudes (A_{max}; mean ± SEM (standard error of the mean)) after bleaching > 90% of rhodopsin in WT (n = 8) and *Awat2*$^{-/-}$ (n = 10) mice. Bleaching was achieved by 35-s illumination with bright 520-nm LED light at time 0. For the rest of the experiment, the mice were kept in darkness and their rod a-wave maximal response and sensitivity were measured periodically with a test flash. Panel **C** shows the raw data presented in panel **B** without normalization to dark-adapted values. **D**, recovery of

normalized scotopic ERG a-wave flash sensitivity (S_f; mean ± SEM) after bleaching > 90% of rod pigment in WT (n = 8) and *Awat2*$^{-/-}$ (n = 10) mice. S_f^{DA} designates the sensitivity of dark-adapted rods. Animals and experimental conditions were the same as in panel **B**. The raw data before normalization to dark-adapted values are shown in panel **E**.

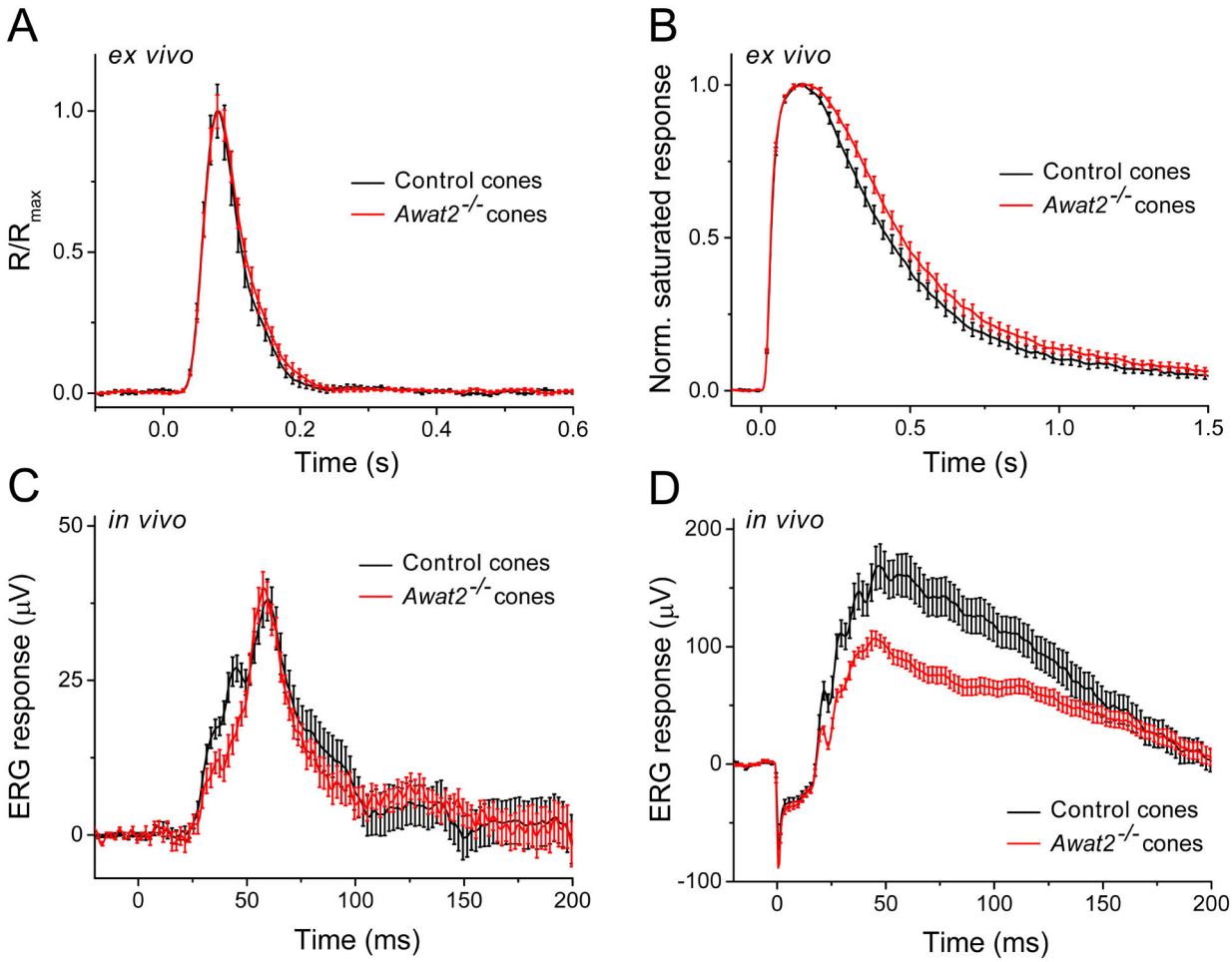

Figure 6 –. Physiological characterization of M-cones in dark-adapted WT and *Awat2*$^{-/-}$ mice.

A, kinetics of cone phototransduction in control (*Gnat1*^{irdr}) and *Awat2*$^{-/-}$/*Gnat1*^{irdr} mice *ex vivo*. Population-averaged (mean ± SEM) dim flash responses to test stimuli of 7.0 × 10^3 photons μm^{-2} (n = 18 for each line) were normalized to maximal response amplitudes (R_{max}) of respective retinas. **B**, comparison of saturated cone responses from control (*Gnat1*^{irdr}) and *Awat2*$^{-/-}$/*Gnat1*^{irdr} animals *ex vivo*. Population-averaged (mean ± SEM) responses to test stimuli of 2.0 × 10^6 photons μm^{-2} (n = 18 for each strain) were normalized to R_{max} of respective retinas. **C**, kinetics of cone ON bipolar cell driven ERG b-wave responses in control (*Gnat1*^{irdr}) and *Awat2*$^{-/-}$/*Gnat1*^{irdr} mice *in vivo*. Population-averaged (mean ± SEM) dim flash responses to test stimuli of 0.24 cd·s m^{-2} (n = 18 for WT, n = 20 for mutant) are shown. **D**, comparison of cone ERG responses (containing both negative a-wave and positive b-wave) in control (*Gnat1*^{irdr}) and *Awat2*$^{-/-}$/*Gnat1*^{irdr} mice *in vivo*. Population-averaged (mean ± SEM) bright flash responses to test stimuli of 700 cd·s m^{-2} (n = 18 for control mice, n = 20 for mutant) are presented.

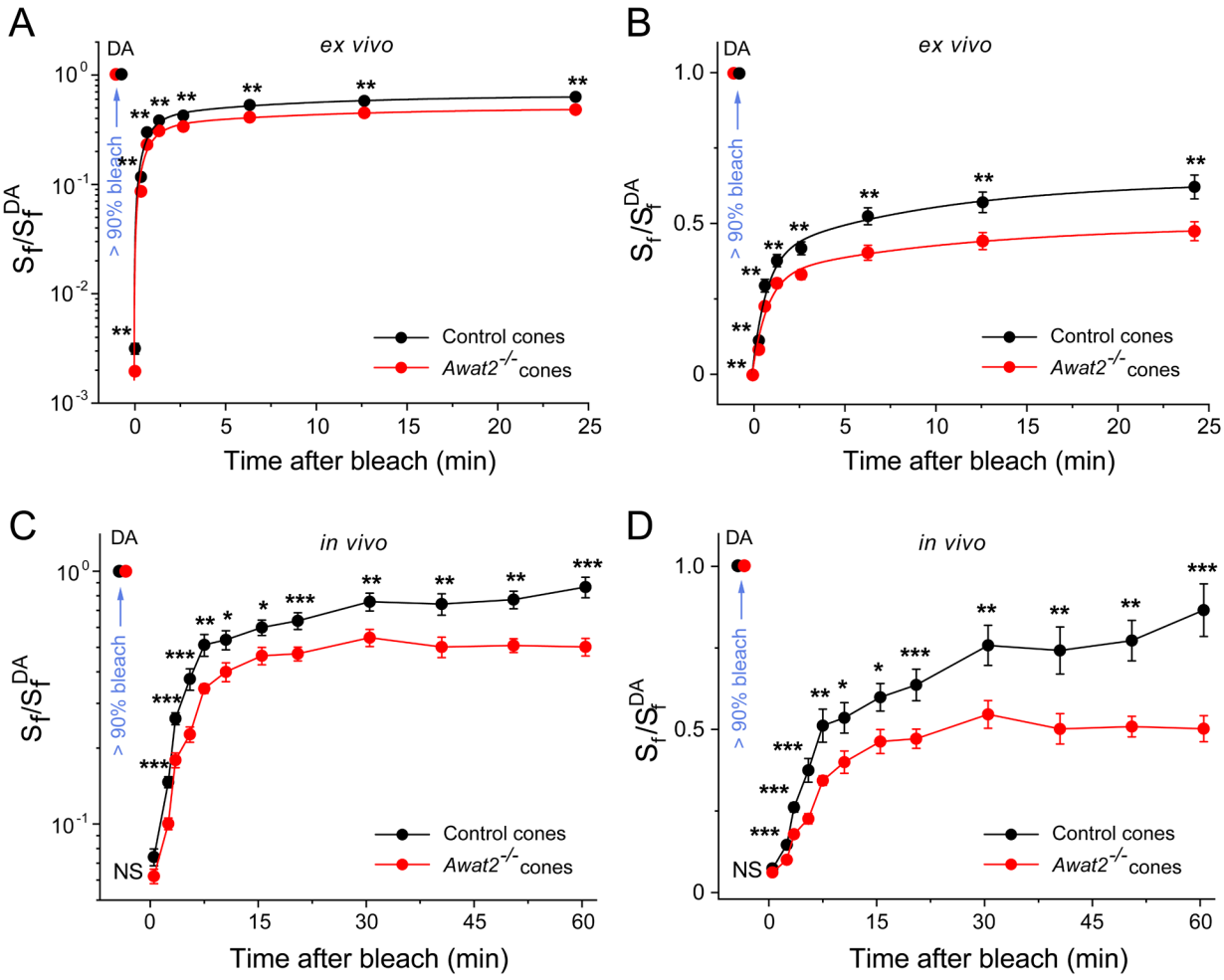

Figure 7 –. Suppressed M-cone dark adaptation in AWAT2-deficient mice.

A, *ex vivo* recovery of normalized cone ERG a-wave flash sensitivity (S_f) in isolated retinas of control (*Gnat1*^{irdr}) (n = 17) and *Awat2*$^{-/-}$/*Gnat1*^{irdr} (n = 19) animals after bleaching > 90% of cone pigment at time 0 with 505 nm LED light. For the rest of the experiment, the retinas were kept in darkness and their cone sensitivity was measured periodically with a test flash. Averaged data were fitted with double-exponential functions that yielded the recovery time constants of 0.77 min and 9.6 min for control and 0.82 min and 10.8 min for mutant mice. The final level of S_f recovery by 25 min post-bleach was lower by ~23% in *Awat2*$^{-/-}$/*Gnat1*^{irdr} mice. S_f^{DA} denotes the sensitivity of dark-adapted (DA) cones. Statistical significance of the data between control and mutant mice is represented by $^{**}p < 0.01$ (all points). Panel **B** represents data shown in panel **A** in a linear scale for S_f/S_f^{DA}. **C**, *in vivo* recovery of normalized photopic ERG b-wave flash sensitivity (S_f; mean ± SEM) in control (*Gnat1*^{irdr}) (n = 18) and *Awat2*$^{-/-}$/*Gnat1*^{irdr} (n = 20) mice after bleaching > 90% of cone pigment at time 0 with 520 nm LED light. For the rest of the experiment, the mice were kept in darkness and their cone b-wave sensitivity was measured periodically with a test flash. S_f^{DA} designates the sensitivity of dark-adapted cones. **D**, data from panel **C** represented

on a linear scale. Statistical significance of the data between control and mutant mice is represented by *$p < 0.05$, **$p < 0.01$, or ***$p < 0.001$. NS – not significant ($p > 0.05$).